Zehra Ese*, Daniel Erni, and Waldemar Zylka

Accuracy of CT numbers and electron density calibration for mixtures of materials with low and high-atomic number

https://doi.org/10.1515/cdbme-2023-1103

Abstract: In computed tomography (CT) materials with high-atomic number Z cause image artefacts, thus, errors in CT numbers given in Hounsfield Units (HU). Also, the conventional HU scale (CHU) implemented in CT scanners is truncated, i.e., it does not cover high-Z materials. These restrictions lead to incorrect mapping of CT numbers to electron density, which are used in radiotherapy (RT) treatment planning systems (TPS). Even analytical conversion methods are only permissible for tissue-equivalent materials. In terms of HU-to-density conversion in RT TPS, we investigated the CT numbers of material mixtures up to $Z \leq 29$ at the CHU and an extended-HU (EHU) scale, respectively, and quantify the systematic errors of image artefacts. In [1] the feasibility of a stoichiometric analytical calibration method were analyzed for metals and adapted for higher accurcy, for energies of $80\,\mathrm{kV}$ and $120\,\mathrm{kV}$. In this work, we add results for $100\,\mathrm{kV}$ and $140\,\mathrm{kV}$ to cover the wide diagnostic range. The CT numbers are effected by physical and machine-based properties and depend strongly on the energy, e.g., for Cu a HU difference of $6\,171\,\mathrm{HU}$ at $80\,\mathrm{kV}$ and $140\,\mathrm{kV}$ occured. The analytical calibration parameters change with energy by a factor between 2 and 10 depending on the physical process. Although for high-Z materials our calibration procedure remains in conflict with rigorous physics [2], it offers an improved and a practical way to predict electron densities from CT numbers.

Keywords: computed-tomography calibration, extended Hounsfield scale, stoichiometric calibration, radiotherapy

***Corresponding author: Zehra Ese,** Faculty of Electrical Engineering and Applied Natural Science, Westphalian University, Campus Gelsenkirchen, Germany, and General and Theoretical Electrical Engineering (ATE), Faculty of Engineering, University of Duisburg-Essen, and CENIDE – Center for Nanointegration Duisburg-Essen, D-47048 Duisburg, Germany, e-mail: zehra.ese@stud.uni-due.de

Daniel Erni, General and Theoretical Electrical Engineering (ATE), Faculty of Engineering, University of Duisburg-Essen, and CENIDE – Center for Nanointegration Duisburg-Essen, D-47048 Duisburg, Germany

Waldemar Zylka, Faculty of Electrical Engineering and Applied Natural Science, Westphalian University, Campus Gelsenkirchen, Germany

1 Introduction

Dose calculations in RT TPS are based on the interaction processes of radiation particles with materials, characterized by the electron density ρ^e [3]. In clinical practice, CT numbers are used to obtain ρ^e, whose accuracy limit the precision of dose calculation. Commercial CT scanners use a conventional HU-scale, which is suitable for human body tissues but limited for high-Z materials, such as metals or medical implants. For mapping high-Z materials, an EHU-scale has proven useful in [4]. In this work, we investigate the CT numbers of material mixtures up to $Z \leq 29$ at the CHU and EHU scale at various energies and quantify the systematic errors due to image artefacts.

A stoichiometric calibration method, introduced in [5], is an analytical approach to obtain ρ^e of a material mixture. This method is based on the factorization of the cross–section in terms of functions of Z and the energy E. Since the exact physics formulas are hard to compute, particularly for material mixtures and polychromatic X–ray spectra, an empirical parametrization procedure based on factorization is used for tissue-equivalent materials in the diagnostic energy range $E = 80 - 140\,\mathrm{kV}$ [6]. This approach is practical, since the coefficients can be fitted to measured CT numbers and thus the spectral X-ray energy distribution can be taken into account. Once fitted to a calibration–material set, one is able to predict the electron density or CT numbers of other materials.

Previously, we investigated energies of $E = 80\,\mathrm{kV}$ and $E = 120\,\mathrm{kV}$ for mixtures up to $Z \leq 29$ [1]. All assumptions imposed on the stoichiometric calibration were systematically reviewed, the validity and accuracy were investigated.. In this work, we extend these results to $E = 100\,\mathrm{kV}$ and $E = 140\,\mathrm{kV}$, to cover the diagnostic energy range.

2 Materials and Methods

On CT images the spatial distribution of linear X–ray attenuation coefficients μ of tissues is reconstructed and converted into CT numbers H by means of the linear function $H(u) = su + i$, where $u = 1000\mu/\mu_w$ is dimensionless with

μ_w the attenuation coefficient of water, s is the slope and i the intercept in the DICOM (Digital Imaging and Communications in Medicine) storage. The unit of H, s and i are given by HU. By setting $s = 1\,\text{HU}$ and $i = -1\,000\,\text{HU}$ the standard CHU scale interval of $[-1\,024\,\text{HU};\ +3\,071\,\text{HU}]$ is found, which suits biological tissues but produces errors for high-Z materials.

We acquired CTs of a Gammex-Tomo-467 tissue characterization phantom with 13 materials and four metallic coin shaped samples made of Al ($Z = 13$), Cr ($Z = 24$), Ti ($Z = 22$) and Cu ($Z = 29$) being in a water phantom [1, 4]. The densities and elemental composition of all materials were known. Both phantoms were acquired using the $80, 100, 120$ and $140\,\text{kV}$ spectra of the Siemens SOMATOM® Force CT scanner. Images were reconstructed by filtered-back projection on both HU scales, respectively. The mean CT number $\overline{H}$, the variance and error of the mean within a defined region of interest (ROI) for each material, calculated by $\overline{H} := \frac{1}{N}\sum_{i=1}^{N} H_i$, $S = +(\frac{1}{N-1}\sum_{i=1}^{N}(H_i - \overline{H})^2)^{1/2}$ and $\Delta\overline{H} := \frac{S}{\sqrt{N}}$, with N representing the number of total CT numbers were determined and plotted in Fig. 1. In order to evaluate the influence of image artefacts on the measured CT numbers caused by metals, HU profiles were obtained along the metal samples for each energy and compared in Fig.2.

In [1], we applied the stoichiometric calibration for tissue equivalent materials and mixtures of $Z \leq 29$. The linear attenuation coefficient $\mu(S, Z_i)$, is defined by ρ^e and the total X–ray cross–section per atom σ_i, which is a sum of cross–sections of photoelectric absorption, $\sigma^{ph}(E, Z)$, coherent scattering, $\sigma^{coh}(E, Z)$, and incoherent scattering, $\sigma^{incoh}(E, Z)$, in the energy range of $80 - 140$ kV. The linear attenuation coefficient averaged over the X–ray spectra $S(E)$ is denoted by $\widehat{\mu}(S, Z_i)$ and can be parametrized in Z by spectrum dependent expansion coefficients $\widehat{K}^{\circ}(S)$, where $\circ$ denotes one of the physical processes mentioned above [2]. The parametrization coefficients must be determined for the particular spectrum $S(E)$ by a fitting procedure to CT numbers of calibration materials with known densities and elemental compositions. As in [3], $\widehat{K}^{\circ}$ of the calibration material are normalized by $\widehat{K}_w^{incoh}$ of water forming $\widehat{k}^{\circ}(S) = \widehat{K}^{\circ}/\widehat{K}_w^{incoh}$ to be obtained from

$$\frac{\widehat{\mu}}{\widehat{\mu}_w}(\widehat{k}^{ph}, \widehat{k}^{coh}) = \frac{\rho^e}{\rho_w^e}\left(\frac{\widehat{k}^{ph}\widetilde{Z}^{p-1} + \widehat{k}^{coh}\widetilde{Z}^{q-1} + 1}{\widehat{k}^{ph}\widetilde{Z}_w^{p-1} + \widehat{k}^{coh}\widetilde{Z}_w^{q-1} + 1}\right) \quad (1)$$

with $\widetilde{Z}$ the weighted (effective) atomic number, $p = 4.62$ and $q = 2.86$ exponents taken from [6].

Once the scanner–specific coefficients $\widehat{k}^{\circ}$ are known for each energy spectrum, the values of the relative electron density $\rho_{rel}^e = \rho^e/\rho_w^e$ of other materials and mixtures with known elemental composition can be computed and look–up–tables for X–ray RT created using Eq. (1).

All materials, were subdivided into two segments (I and II) separated by ρ_{rel}^s, representing SB3 cortical bone, which is a Gammex-Tomo-467 phantom material. The least square fit was done separately in each segment. Using $\rho_{rel}^s = 1.69$ was proven to provide an accurate fit [1].

3 Results

The mean CT numbers and their errors measured at the energies $80, 100, 120$ and $140\,\text{kV}$ on both HU scales are compared in Fig. 1. On both HU scales, the tissue equivalent materials including Al, are measured the same numbers. The CT numbers of Ti, Cr and Cu saturate on the CHU skale's maximum with $+3017\,\text{HU}$. Increasing X–ray energy results in a smaller CT number for each material, while this effect increases with increasing material density, which is shown for the tissue equivalent materials on the CHU and for all materials including

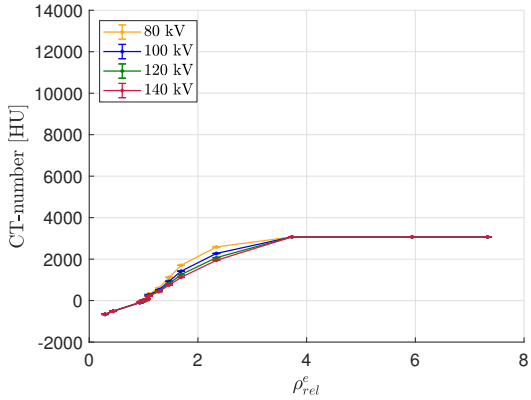

(a) Conventional HU scale (CHU)

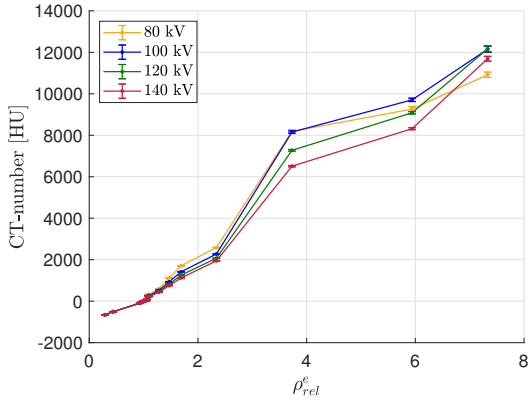

(b) Extended HU scale (EHU)

Fig. 1: Comparison of CT numbers of tissue equivalent and metals, mapped on (a) CHU and (b) EHU scale at $80, 100, 120$ and $140\,\text{kV}$, respectively.

metals on the EHU scale. With increasing metal density, however, the energy dependence of the CT numbers apparently increases. The CT numbers of the metals measured at 80 kV are particularly striking. For Cr the CT number at 80 kV is lower than at 100 kV, with 9 263 HU and 9 708 HU respectively. For Cu this effect becomes even stronger, the CT number at 80 kV (10 916 HU) is lower than at 100, 120 and 140 kV (12 150 HU, 12 168 HU, 11 690 HU).

The H profiles in Fig. 2 represent the CT number distribution along the transversal cross-section of the metals. For each metal, the H profiles were recorded at a X–ray energy of 80, 100, 120 and 140 kV, respectively. For Al, shown in Fig. 2 (a), an almost homogeneous H distribution is shown for all energies. With increasing atomic–number Z, the CT numbers decrease almost exponentially towards the centre of the metal, which is identified as cupping artefact and particularly caused by beam hardening effects. This effect shows a material and energy dependence, gaining strength with increasing atomic–number Z. For Cu, CT number differences, between the maximum and minimum, of 14 699 HU at 80 kV and 8 528 kV at 140 kV were measured. For Cr and Ti, numbers of 8 142 HU, 4 632 HU at 80 kV and 2 830 HU and 1 835 HU at 140 kV, respectively, are obtained. Also, we observe the higher the H difference at the water-metal interface, the more the CT number of water is under-represented. This effect is amplified with decreasing energy.

At 80, 100, 120 and 140 kV, respectively, the mean CT number H and its error σ_{err} are determined from images and represented in Fig. 1. $\widehat{k}^{\circ}$ values were calculated for segments separated by the point $\rho^{s}_{rel} = 1.69$. In Figure 3 the measured HU values and those calculated by the stoichiometric calibration method, i.e. $\frac{\widehat{\mu}}{\widehat{\mu}_w}(\widehat{k}^{ph}, \widehat{k}^{coh})$, are displayed for 100 and 140 kV. All $\widehat{k}^{\circ}$ values calculated for $\overline{H}$ and $\overline{H} \pm \sigma_{err}$ are given in Tab. 1.

For materials in the range $\rho^{e}_{rel} = 3.7 - 8.0$ a considerable mismatch between measured and calculated CT numbers is observed. This cannot be explained by the statistical errors σ_{err} and must be seen as a systematic error steaming, e.g. from CT image artefacts and an incorrect parametrisation of the cross–section.

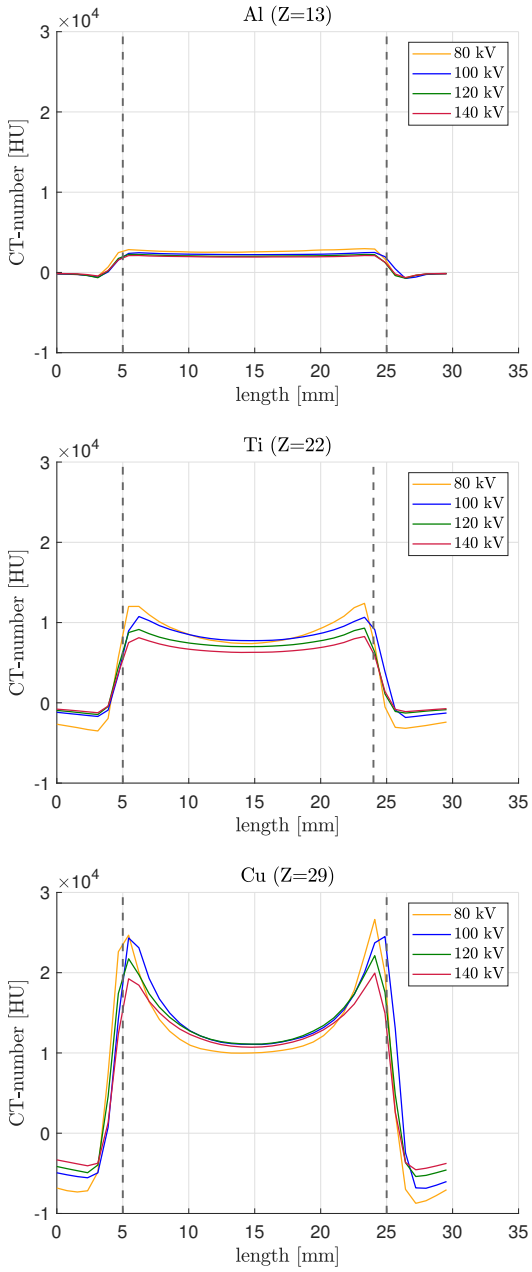

Fig. 2: H profiles recorded for three metals Al, Ti, Cu, respectively at tube voltages of 80, 100, 120 and 140 kV. The object position is outlined.

4 Discussion

The total cross–section $\sigma_i(E, Z_i)$, consequently the CT numbers are influenced by the beam energy, the X-ray spectrum and by the technical composition of the X–ray system. According to the general definition $H(u)$, CT numbers increase with increasing atomic number Z and decreasing energy. In Figure 1(b), however, slightly changing distribution of CT numbers for the metals are observed. CT number differences for the respective metals become smaller with increasing material density at variable energy. At 80 kV compared to the other energies, the smallest CT number for Cu is shown, which expected to be the highest number. There are no absorption edges for the metals Cr and Cu, which could explain this behaviour. Rather, it is due to the saturation effect of the CT detector. When the photon flux at the detector is low, e.g. after very strongly absorbing materials, statistical components gain in-

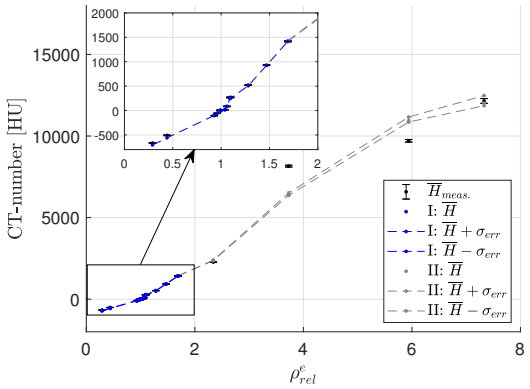

(a) $E = 100\,\mathrm{kV}$

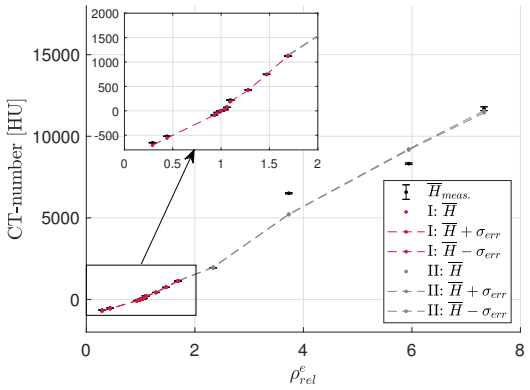

(b) $E = 140\,\mathrm{kV}$

Fig. 3: Measured and calculated CT numbers at $100\,\mathrm{kV}$ and $140\,\mathrm{kV}$ for tissue equivalent materials and metals versus relative electron density ρ^e_{rel}. Measured CT numbers are displayed with the error of the means.

creasing influence, especially due to the unavoidable quantum statistics of the photons. Saturation can set-in early at low voltages that the CT numbers are smaller than at higher energies, which is basically the photon starvation artefact [7]. Despite these observations, the EHU scale provides reliable CT numbers for metals than the CHU scale.

The observations in Fig. 2 show that the determined CT numbers strongly depend on the positioning and size of the chosen ROI. If the ROI is set to the central area of the metal, the CT numbers will be under-estimated. An extension of cupping artefact corrections beyond water could be beneficial.

5 Conclusion

The computation of CT numbers of high-Z materials from CT images is susceptible to artefacts, caused among others by beam hardening and scattered radiation. Even if the statistical error is small, the systematic error due to that artefact requires additional quantification. The applicability of the stoichiometric calibration based on parametrization from [3] is limited in the presence of high-Z materials and remains in conflict with rigorous physics and must be replaced by an improved expression [1]. However, once the calibration was done for a set of materials, one is able to predict the electron density of CT numbers of other materials, which might be reduce the effort of CT acquisitions and determination of CT numbers associated with the handling of artefacts. Therefore, in Tab. 1 we delivered the $\widehat{k}^{\circ}$ values measured for a range of energies.

Tab. 1: Parameters $\widehat{k}^{ph}$ and $\widehat{k}^{coh}$ for different X–ray energies. I and II indicates the two segments separated by ρ^s_{rel} on which the least square fit was done separately.

***E* [kV]**	***HU***			
	$\widehat{k}^{ph}_{\mathrm{I}}$ $(\mathrm{x}\,10^{-3})$	$\widehat{k}^{coh}_{\mathrm{I}}$ $(\mathrm{x}\,10^{-5})$	$\widehat{k}^{ph}_{\mathrm{II}}$ $(\mathrm{x}\,10^{-3})$	$\widehat{k}^{coh}_{\mathrm{II}}$ $(\mathrm{x}\,10^{-6})$
80	-0.11	5.15	10.30	-22.00
100	-0.78	3.85	9.60	-18.60
120	-1.00	3.11	6.90	-12.20
140	-1.10	2.53	4.90	-7.96

Author Statement

The author state no funding involved. Authors state no conflict of interest.

References

[1] Ese Z, Zylka W. Extension of the Stoichiometric Calibration of CT Hounsfield values to Metallic Materials. Current Directions in Biomedical Engineering 2020;6(3):526-529.

[2] Jackson D F, Hawkes D J. X-ray attenuation coefficients of elements and mixtures. Elsevier - Physics Reports 1981;70(3):169-233.

[3] Schneider W, Bortfeld T and Schlegel W. Correlation between CT numbers and tissue parameters needed for Monte Carlo simulations of clinical dose distributions. Physics in Medicine and Biology 2000;45:459–478.

[4] Ese Z, Qamhiyeh S, Kreutner J, Schaefers G, Erni D, Zylka W. CT Extended Hounsfield Unit range in radiotherapy treatment planning for patients with implantable medical devices. Springer Nature Singapore IFMBE Proc 2019;68(3),599-603.

[5] Schneider U, Pedroni E, Lomax A. The calibration of CT Hounsfield units for radiotherapy treatment planning. Physics in Medicine and Biology 1996;41:111-124.

[6] Rutherford R A, Pullan B R, Isherwood I. Measurement of effective atomic number and electron density using an EMI scanner. Neuroradiology 1976;11(1):15-21.

[7] Mori I, Machida Y, Osanai M and Iinuma K. Photon starvation artifacts of X-ray CT: their true cause and a solution. Radiol Phys Technol. 2013 Jan;6(1):130-41.